https://doi.org/10.5194/egusphere-2022-530
Preprint. Discussion started: 29 June 2022
© Author(s) 2022. CC BY 4.0 License.

Spatio-temporal synchronization of heavy rainfall events triggered by atmospheric rivers in North America

Sara M. Vallejo-Bernal[1,2], Frederik Wolf[1], Niklas Boers[1,3,4], Dominik Traxl[1], Norbert Marwan[1,2], and Jürgen Kurths[1,2]

[1]Research Domain IV - Complexity Science, Potsdam Institute for Climate Impact Research (PIK) – Member of the Leibniz Association, Potsdam, Germany
[2]Institute of Geoscience, University of Potsdam, Germany
[3]Earth System Modelling, School of Engineering & Design, Technical University of Munich, Germany
[4]Global Systems Institute and Department of Mathematics, University of Exeter, UK

Correspondence: Sara M. Vallejo-Bernal (vallejo.bernal@pik-potsdam.de)

Abstract. Atmospheric rivers (ARs) are filaments of extensive water vapor transport in the lower troposphere, that play a crucial role in the distribution of water, but can also cause natural and economical damage by facilitating heavy rainfall. Here, we investigate the large-scale spatio-temporal synchronization patterns of heavy rainfall over the western coast and the continental regions of North America (NA), during the period from 1979 to 2018. In particular, we utilize event synchronization and a complex network approach incorporating varying delays to examine the temporal evolution of spatial patterns of heavy rainfall events in the aftermath of land-falling ARs. For that, we employ the SIO-R1 catalog of ARs that land-fall over the western coast of NA, categorized in terms of strength and persistence on an AR-intensity scale which varies from category 1 to 5, along with daily rainfall estimates from the ERA5 reanalysis with $0.25°$ spatial resolution. Our analysis reveals a cascade of synchronized heavy rainfall events, triggered by ARs of category 3 or higher: in the first 3 days after the first day of an AR strike, rainfall events mostly occur and synchronize along the western coast of NA. In the subsequent days, moisture can be transported to central and eastern Canada and cause synchronized but delayed heavy rainfall there. Furthermore, we assess the robustness of our findings by studying an additional AR detection method. Finally, analyzing the anomalies of integrated water vapor transport, geopotential height, upper-level meridional wind, and rainfall, we find atmospheric circulation patterns that are consistent with the spatio-temporal evolution of the synchronized heavy rainfall events. Understanding and revealing the effects of ARs in the rainfall patterns over NA will lead to better anticipating the evolution of the climate dynamics of the region in the context of a changing climate.

1 Introduction

Atmospheric rivers (ARs) are channels of enhanced water vapor flux that transport moisture over thousands of kilometres, often from the tropics to the mid-latitudes of both hemispheres, where they land-fall and cause copious rainfall (e.g. (Zhu and Newell, 1998; Ralph and Dettinger, 2011; Baggett et al., 2017; Eiras-Barca et al., 2018; Mundhenk et al., 2018; Shields et al., 2018; Ralph et al., 2019; Payne et al., 2020; O'Brien et al., 2022)). Located in the lower troposphere, ARs can persist from

https://doi.org/10.5194/egusphere-2022-530
Preprint. Discussion started: 29 June 2022
© Author(s) 2022. CC BY 4.0 License.

several hours to several days and play a crucial role in the global water cycle (Neiman et al., 2008), the Arctic water influx (Baggett et al., 2016), and can cause heavy rainfall (Neiman et al., 2008; Krichak et al., 2015). Due to the increase of water vapor, it is to be expected that their frequency (Gao et al., 2015; Hagos et al., 2016) and intensity (Payne et al., 2020) will increase in the next decades in the context of ongoing climate change.

Further motivated by their high economical impacts, occurrences of ARs have been studied intensively in the last decade, especially on the western coasts of North America (NA) and in Europe (Smith et al., 2010; Dettinger et al., 2011; Newman et al., 2012; Lavers and Villarini, 2013; Warner et al., 2015; Krichak et al., 2015; Shields and Kiehl, 2016; Ramos et al., 2016; Baggett et al., 2017; Shields et al., 2018; Mundhenk et al., 2018; Eiras-Barca et al., 2018; Ralph et al., 2019; Lora et al., 2020; Guirguis et al., 2020; Huang et al., 2021; O'Brien et al., 2022)). ARs typically form at the front of a mid-latitude cyclone and cause rainfall due to an ascent of air masses by a warm conveyor belt intersecting with orography (Zhang et al., 2019; Sharma and Déry, 2020). Given that ARs land-falling at the western coast of NA frequently accumulate their moisture over the central Pacific, and that the exact location of the cyclonic storms heavily influences the location of the AR, AR frequency and intensity are modulated by the Madden-Julian Oscillation (MJO), the Quasi-Biannual Oscillation (QBO), the El-Niño Southern Oscillation (ENSO) and the Pacific Decadal Oscillation (PDO) (Baggett et al., 2017; Mundhenk et al., 2018; Zhou et al., 2021). Along the dryer southwestern coast of NA, ARs play an essential role in the water supply (Smith et al., 2010; Dettinger et al., 2011). There, the less intense ARs are beneficial and act as central sources of fresh water by facilitating rainfall, whereas intense ARs cause large natural and economical damage (Waliser and Guan, 2017; Corringham et al., 2019; Gershunov et al., 2019; Ralph et al., 2019).

Although there has been an increasing effort in characterizing and predicting AR strikes along the North American west coast by presenting comprehensive analyses of drivers and properties of AR-related land-fall, the spatio-temporal synchronization patterns of heavy rainfall induced by ARs have not yet been studied. Here, we understand spatio-temporal synchronization as a relation between time series at different locations, where events in one time series measured at a location are significantly followed or preceded by events at another. Such an assessment has led, among other findings (see e.g. (Boers et al., 2013; Stolbova et al., 2014; Agarwal et al., 2019; Wolf et al., 2020b)), to forecasting rainfall events in the Eastern Central Andes (Boers et al., 2014) and identifying Rossby waves as one controlling mechanism of heavy rainfall worldwide (Boers et al., 2019). In this light, it has not been examined to what extent ARs are accompanied by characteristic synchronization patterns of heavy rainfall. Additionally, we study the lag-dependent spatial impact of ARs hitting the western coast. We utilize two different catalogs with different AR-tracking schemes to address these specific research questions and to elaborate on the issues explained and examined by the ARTMIP project (Shields et al., 2018; Rutz et al., 2019; O'Brien et al., 2022), which showed that observations are often catalog-dependent. Both catalogs considered here, the SIO-R1 product which was recently published by Gershunov et al. (2017) and a self-constructed one which is based on the IPART algorithm Xu et al. (2020), cover the period between 1979 and 2018. Based on the occurrence of ARs, we perform time series and complex network analyses evaluating the spatio-temporal correlation of heavy rainfall events and their relation to ARs. To interpret our results, we furthermore study the corresponding climatologies of different variables such as upper-level meridional wind and geopotential height at 500 hPa.

https://doi.org/10.5194/egusphere-2022-530
Preprint. Discussion started: 29 June 2022
© Author(s) 2022. CC BY 4.0 License.

The paper is structured as follows: first, we introduce the employed data sets and methods, in particular the characteristics of the two AR catalogs, the ERA5 reanalysis and the event synchronization (ES) and complex network techniques. Second, we conduct an ES-based assessment of the temporal correlation between AR strikes and heavy rainfall events for different lags. Having revealed different temporal scales at which AR-related heavy rainfall events occur, we set up two climate networks based on rainfall events taking place at different lags. Finally, we study composites of integrated water vapor transport, geopotential height, upper-level meridional wind, and rainfall for the times during which we identified features of synchronized heavy rainfall and we discuss our findings in the context of the guiding climatology.

2 Data and Methods

2.1 Data sets

For our analyses, we utilize data from the ERA5 reanalysis (ECMWF, 2021). All ERA5 data sets are available on a longitude-latitude grid with a spatial resolution of $0.25° \times 0.25°$. We construct daily estimates for integrated water vapor transport (IVT), geopotential height at 500 hPa, meridional wind at 250 hPa, and rainfall by considering the daily mean of the hourly data sets for the period between 1979 and 2018.

To examine the synchronization of heavy rainfall, we especially consider the 95^{th} percentile thresholds of the daily precipitation estimates. Only days exceeding 1 mm of total rainfall are used for computing the percentiles.

In addition to the ERA5 reanalysis data set, we use the SIO-R1 catalog of ARs by Gershunov et al. (2017). It includes ARs land-falling at the western coast of NA and was constructed using Lagrangian backtracking of high values of two variables, namely the vertically integrated horizontal vapor transport (IVT), and the vertically integrated water vapor (IWV), on a longitude-latitude grid with a resolution of $2.5° \times 2.5°$. The catalog features a 6-hourly time series indicating whether an AR has been active, the grid cells covered by the AR, and the IVT over the grid cell along the coast where the AR land-falls. We transform the 6-hourly catalog into a daily one by considering each day with at least one (of the four) 6-hourly time steps with an AR present as an *AR-day*. Approximately one-third of all days of the considered period are AR-days (at least one AR active somewhere in the spatial domain covered by the catalog). These days are distributed relatively equally over the different years but are strongly seasonally clustered in boreal autumn and winter.

Furthermore, we create an additional catalog of ARs with features similar to the SIO-R1 catalog but using the Image-Processing-based Atmospheric River Tracking (IPART) algorithm (Xu et al., 2020). As opposed to conventional detection methods that rely on thresholding of IVT and/or IWV fields (for instance the detection algorithm of the SIO-R1 catalog), IPART implements the detection task from a spatio-temporal scale perspective and is, therefore, free from magnitude thresholds. The advantage of IPART's approach is that it negates the implicit assumption of thresholding approaches that the atmospheric moisture level stays unchanged throughout the analysis period. As input to the IPART algorithm, we use IVT-fields of the ERA5 reanalysis data set re-gridded to a spatial resolution of $0.75° \times 0.75°$ and a temporal resolution of 6 hours. The parameters passed to the different steps of the IPART algorithm are summarized in Table A1 in appendix A. We transform the 6-hourly product into a daily one in the same manner as described for the SIO-R1 catalog.

https://doi.org/10.5194/egusphere-2022-530
Preprint. Discussion started: 29 June 2022
© Author(s) 2022. CC BY 4.0 License.

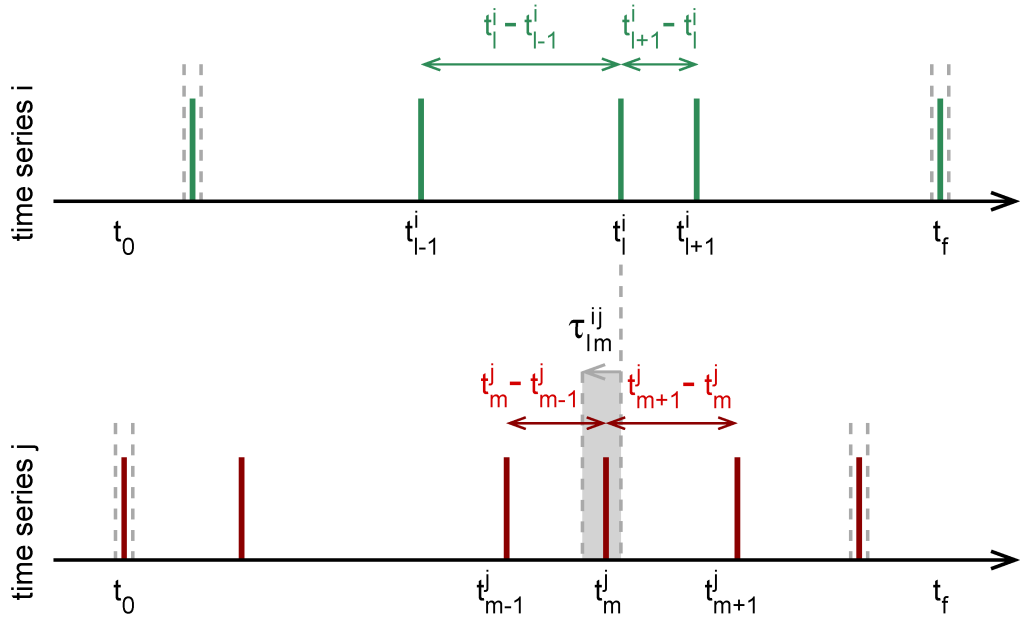

Figure 1. Schematic sketch illustrating event synchronization (ES). Shown is a pair of time series (i,j) and an exemplary computation of the dynamic coincidence interval τ^{ij}_{lm}. Additionally, the first and last events which are not considered for ES are marked by vertical grey lines.

2.2 Event Synchronization (ES)

Event synchronization (ES), as initially introduced by Quiroga et al. (2002), is a method to quantify the synchronization of events in a pair of time series. While ES has been originally proposed for analyzing spike trains in electroencephalographic time series, ES is nowadays an established tool employed to construct functional climate networks (Malik et al., 2012; Boers et al., 2013, 2019; Ozturk et al., 2019; Wolf et al., 2020a).

Using ES, two events l and m in time series describing observations made at locations i and j at times t^i_l and t^j_m are considered *synchronized* if and only if they occurred within the *local (dynamical) coincidence interval* τ^{ij}_{lm} (Quiroga et al., 2002)

$$\tau^{ij}_{lm} = \frac{1}{2}\min\left\{t^i_{l+1} - t^i_l, t^i_l - t^i_{l-1}, t^j_{m+1} - t^j_m, t^j_m - t^j_{m-1}\right\}. \tag{1}$$

See Fig. 1 for an illustration of the computation of the dynamic coincidence interval τ^{ij}_{lm}. This dynamical lag allows us to consider events in more densely and more sparsely occupied parts of the time series in an adaptive and automated manner.

To avoid a collapse of the local coincidence interval to $\tau^{ij}_{lm} = \frac{1}{2}$timestep due to sequences of consecutive events, we only consider the first event of all event sequences (cluster-corrected ES) (Boers et al., 2019; Wolf and Donner, 2021).

https://doi.org/10.5194/egusphere-2022-530
Preprint. Discussion started: 29 June 2022
© Author(s) 2022. CC BY 4.0 License.

Then, the synchronization condition reads

$$\sigma_{lm}^{ij} = \begin{cases} 1, & \text{if } 0 < t_l^i - t_m^j \leq \tau_{lm}^{ij}, \\ 0, & \text{otherwise.} \end{cases} \tag{2}$$

Additionally, we can limit the coincidence interval τ_{lm}^{ij} by a maximal value $\tau_{\max}$ to prevent an unrealistically large temporal distance between synchronized events. As the first and last event has no preceding or subsequent event, we exclude them from our computations. Thus, we set $l = 2, 3, ..., s_i - 1$ and $m = 2, 3, ..., s_j - 1$ where s_i and s_j denote the number of events in the time series at location i and j, respectively.

Employing the indicator function (Wolf et al., 2020a)

$$J_{lm}^{ij} = \begin{cases} 1, & \text{if } \sigma_{lm}^{ij} = 1, \sigma_{m,l-1}^{ji} = 0 \text{ and } \sigma_{m+1,l}^{ji} = 0, \\ \frac{1}{2}, & \text{if either } t_l^i = t_m^j \text{ or } \sigma_{lm}^{ij} = 1 \text{ and } (\sigma_{m,l-1}^{ji} = 1 \text{ or } \sigma_{m+1,l}^{ji} = 1), \\ 0, & \text{otherwise,} \end{cases} \tag{3}$$

we calculate the total number of synchronized events by

$$c(i|j) = \sum_{l=2}^{s_i - 1} \sum_{m=2}^{s_j - 1} J_{lm}^{ij}. \tag{4}$$

The indicator function assures that pairs of synchronized events are not considered in both $c(i|j)$ and $c(j|i)$ (Wolf et al., 2020a). Here, $c(j|i)$ indicates the number of synchronized events where an event at i precedes an event at j.

We utilize $c(i|j)$ and $c(j|i)$ to compute the *directed event synchronization strength* as

$$q_{ij} = c(i|j) - c(j|i)\,. \tag{5}$$

In our work, we use this measure to investigate (a) if there is a directed synchronization between ARs and heavy rainfall events and (b) between heavy rainfall events at different locations. For the latter, we use the matrix $\boldsymbol{Q}^{ES}$ (with matrix elements q_{ij}^{ES}) for setting up climate networks (see Sect. 2.3).

2.3 Climate networks

In climate networks, as introduced in former work by Tsonis and Roebber (2004), Tsonis et al. (2006), and Donges et al. (2009), links are placed between nodes based upon some statistical association between the time series associated with these nodes, typically measured at specific spatial locations or grid cells. Here, we utilize ES to assess the spatio-temporal correlation structure of heavy rainfall in NA. For that, we identify the nodes of the network with the gridded time series of the ERA5 reanalysis data and connect the nodes based on their statistical association evaluated by ES. To transform the daily ERA5 rainfall estimates to an event time series, we threshold each time series (located at the grid points) at the 95^{th} percentile. Subsequently, we apply the cluster-corrected ES (Boers et al., 2014; Wolf et al., 2020a) with an upper threshold of the dynamical coincidence interval which is specified in the respective sections.

https://doi.org/10.5194/egusphere-2022-530
Preprint. Discussion started: 29 June 2022
© Author(s) 2022. CC BY 4.0 License.

A network consists of N nodes connected by e edges. The topology of such a network is commonly encoded in the adjacency matrix $\mathbf{A}$ with elements a_{ij} indicating if nodes i and j are connected. In directed networks, as in this work, the adjacency matrix is not symmetric (in contrast to undirected networks), but binary since we do not consider link weights: ($a_{ij} = 1$ if a link points from node j to node i $a_{ij} = 0$ otherwise).

To construct functional climate networks from the resulting matrix $\boldsymbol{Q}^{ES}$, we apply a specifically tailored significance testing scheme. For each pair of time series, we set up a significance test using $1,000$ surrogate time series with the respective numbers of events in each time series. We connect nodes in the network (by setting $a_{ij}^{ES} = 1$) if q_{ij}^{ES} exceeds the 99.5^{th} percentile of the surrogate test distribution (Boers et al., 2019).

To calculate the number of nodes to which node i is connected, we compute the in-degree k_i^{in} as

$$k_i^{in} = \sum_{j=1}^{N} a_{ij}, \tag{6}$$

and the out-degree k_i^{out} as

$$k_i^{out} = \sum_{j=1}^{N} a_{ji}. \tag{7}$$

To aggregate both measures and to especially highlight regions of predominately outgoing (or incoming) connections, we also measure the network divergence

$$d_i = k_i^{out} - k_i^{in} = \sum_{j=1}^{N} a_{ji} - \sum_{j=1}^{N} a_{ij}. \tag{8}$$

3 Results and discussion

3.1 Heavy rainfall events synchronized with strong ARs

As a first step, we investigate where heavy rainfall events occur synchronized to ARs hitting the coast and at which lags. For that, we employ ES and evaluate the synchronization between the AR time series and the time series of the heavy rainfall events at each grid point in the study area. To obtain the latter one, we threshold each rainfall time series at the respective 95th percentile. For the former one, we consider ARs hitting the North American west coast at a latitude $\geq 47.5°$N. Initially, we included all ARs but additional analyses showed that our results are predominantly caused by ARs that land-fall north of $47.5°$N (see appendix A). Moreover, we want to emphasize that our results can be reproduced using an alternative AR catalog (also featured in appendix A). To separate the impact of rather weak ARs from strong ARs, we differentiate between AR categories (classification based on Ralph et al. (2019)) and run the analysis repeatedly, excluding ARs from lower categories.

Figure 2 shows the grid points whose time series of heavy rainfall events have significant ($p < 0.05$) synchronization with the AR time series, given a particular parameter setting of ES and ARs of category 3 or higher. We only observe a significant correlation close to the western coast of NA, which is expected but already implied by findings of previous studies, if we also include ARs of lower categories. Therefore, we have selected this subset for our analysis.

https://doi.org/10.5194/egusphere-2022-530
Preprint. Discussion started: 29 June 2022
© Author(s) 2022. CC BY 4.0 License.

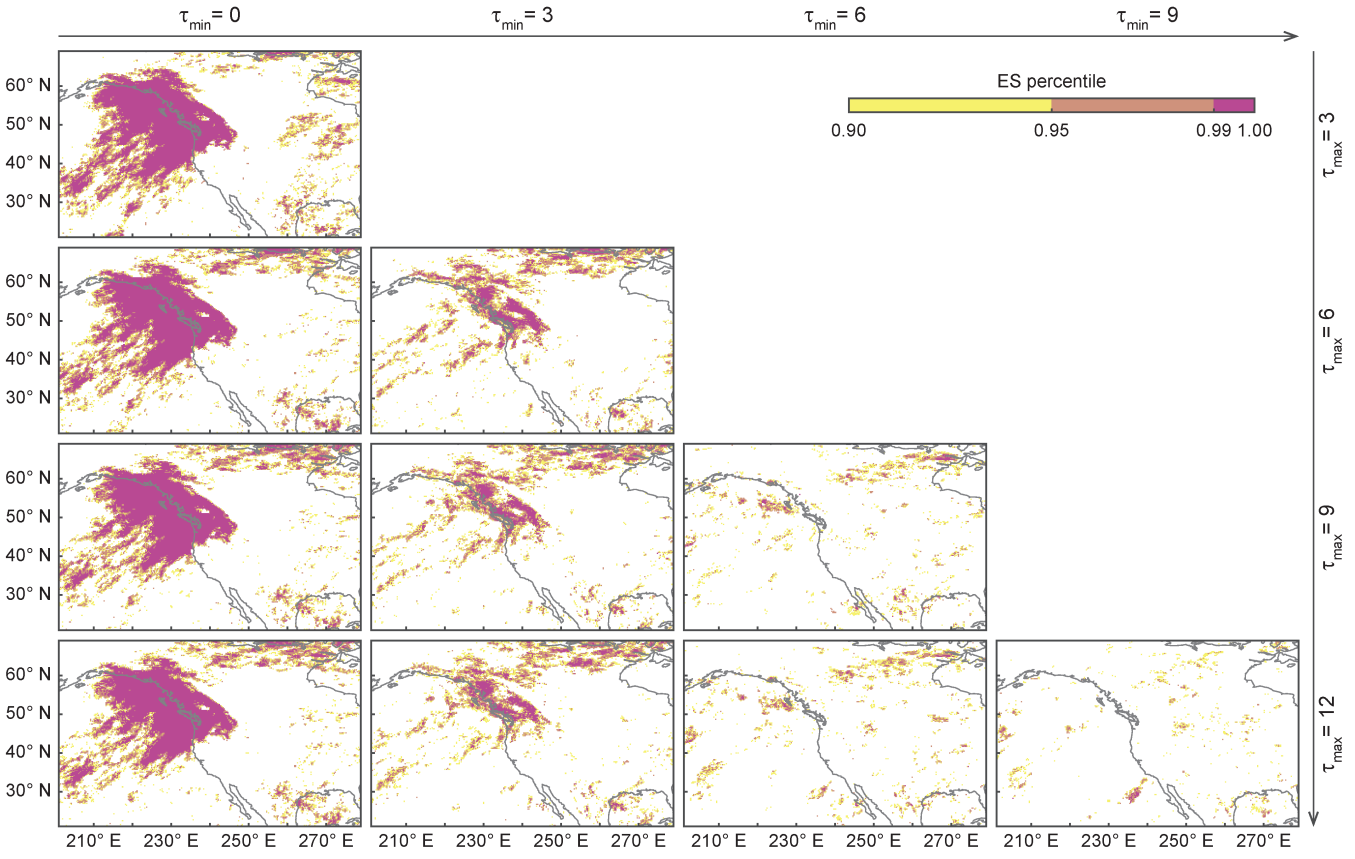

Figure 2. Event synchronization (ES) between time series of heavy rainfall events and the AR time series of the SIO-R1 catalog, considering only ARs of category 3 and higher that land-fell at latitudes $\geq 47.5°$. Different values of τ_{min} and τ_{max} were considered to calculate ES in each panel: τ_{min} increases from left to right and τ_{max} from top to bottom. Note the irregularly spaced color bar: Yellow indicates high, but not significant synchronization between heavy rainfall and ARs of category 3 or higher. Orange indicates significant synchronization with $p < 0.05$ (and ES percentile > 0.95). Pink indicates significant synchronization with $p < 0.01$ (and ES percentile > 0.99).

Consequently, when $\tau_{min} = 0$ (left column), large areas close to the coast show significant correlations as expected. This is caused by heavy rainfall events at the coast that are directly triggered by the ARs. This pattern is not affected by increasing τ_{max}. If events occur in close succession, then a higher possible maximal delay will often not be taken into account and, therefore, the pattern does not change visibly.

When $\tau_{min} = 3$ (second column), the synchronization close to the coast is decreased, as most heavy rainfall falls on the first days after an AR strike. Additionally, most ARs do not persist longer than 3 days. The remaining synchronized events are likely associated with ARs of the higher categories which have a longer persistence. Additionally, we observe a patch of synchronized events in central and eastern Canada. This pattern is strongest when $\tau_{min} = 3$ and $\tau_{max} = 12$ and stands out to a smaller extent for $\tau_{min} = 6$ (third column) and elevated values of τ_{max}

https://doi.org/10.5194/egusphere-2022-530
Preprint. Discussion started: 29 June 2022
© Author(s) 2022. CC BY 4.0 License.

This result implies that in central and eastern Canada, heavy rainfall occurs synchronized (but lagged) to ARs hitting the western coast of NA. We, therefore, suspect that moisture that has been transported to the North American west coast by an AR can be channeled to western and central Canada and also cause heavy rainfall there.

3.2 Synchronization across AR strength

Using ES, we have identified a region of synchronized heavy rainfall events in eastern and central Canada, as explained in the previous section. To further evaluate how the results depend on the selected category criteria, we step-wise exclude ARs of the lower categories for the analysis shown in Fig. 3. Doing this, we reduce the number of events in the AR time series, which heavily affects the outcome of ES. As a result, we find that when we consider all ARs, the signal is present but is less intense and covers a smaller area than previously observed (Fig. 2). The most extensive pattern is found when we take into account ARs of category 3 or higher. Only examining ARs of categories 4 and 5 leads to a vanishing of the pattern, although rainfall anomalies show heavy rainfall in eastern and central Canada for composites based on the days after such strong ARs (see appendix A). We suspect that this is a result of reducing the number of events in the AR time series. Very intense ARs are rare and in this case, the AR time series contains very few events. In other words, the AR time series get too sparse for high ES scores, although heavy rainfall might be always caused by such ARs but likely not *just* by them.

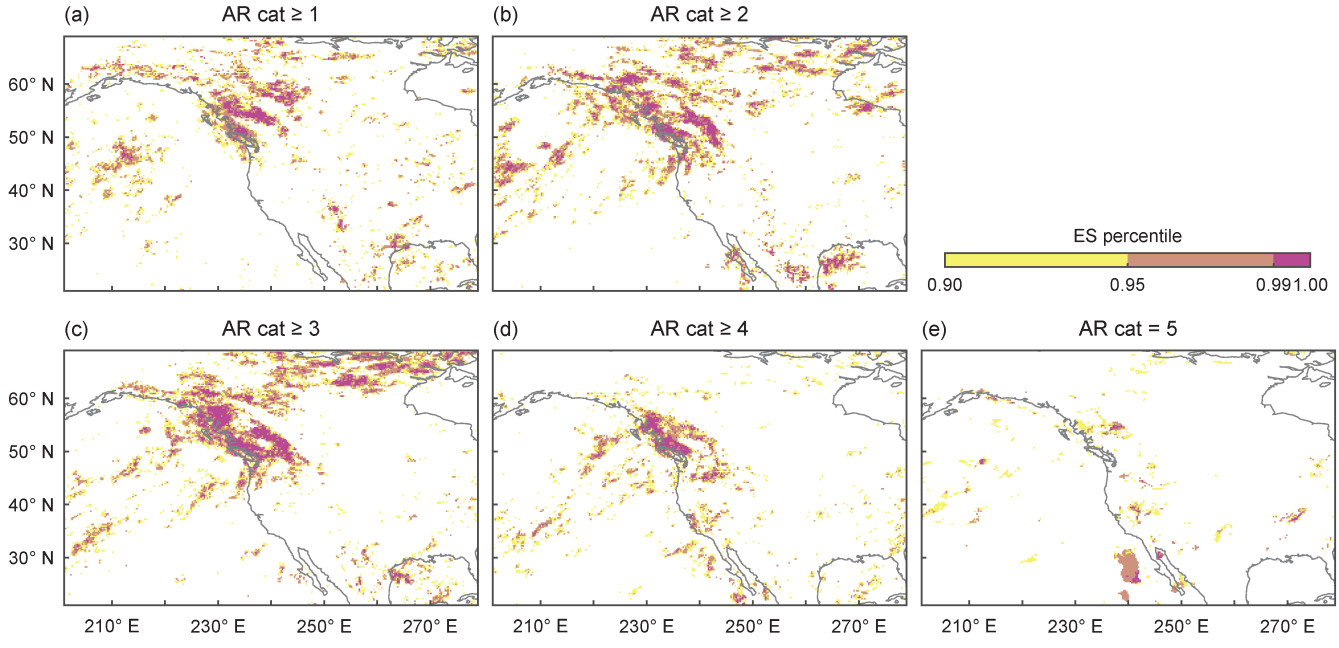

Figure 3. Event synchronization (ES) between time series of heavy rainfall events and the AR time series of the SIO-R1 catalog, considering only ARs that land-fell at latitudes $\geq 47.5°$. ES was calculated with $\tau_{min} = 3$ and $\tau_{max} = 12$. From (a) to (e) the considered lower AR category limit increases: (a) ARs of category 1 and higher e.g. all ARs; (b) ARs of category 2 and higher; rest accordingly. Color bar as in Fig. 2.

https://doi.org/10.5194/egusphere-2022-530
Preprint. Discussion started: 29 June 2022
© Author(s) 2022. CC BY 4.0 License.

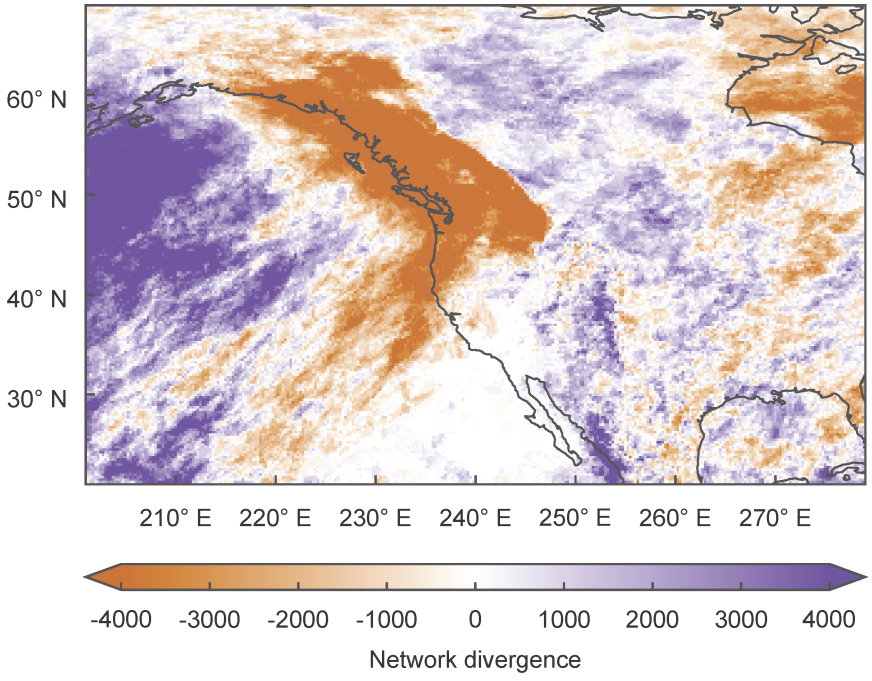

Figure 4. Network divergence based on event synchronization (ES) between heavy rainfall and ARs of category 3 or higher that land-fell at latitudes $\geq 47.5°$ according to the SIO-R1 catalog. We only consider rainfall events that occurred from 0 to 3 days after the land-falling of an AR and we calculate ES with $\tau_{min} = 0$ and $\tau_{max} = 3$. In the network, only nodes with significantly directed event synchronization strength were connected (see Sect. 2 for more details). Purple (orange) colors indicate regions with positive (negative) divergence, i.e. nodes with more outgoing (incoming) connections.

3.3 Network analysis of heavy rainfall during ARs

In the previous sections, we examined the synchronization between heavy rainfall and the singular AR time series (constructed via aggregating ARs land-falling north of $47.5°$ lat). To elaborate further on the concept of synchronized heavy rainfall events, we assess how rainfall at different locations is organized during AR times. For that, we select the days with active ARs of category 3 or higher land-falling north of $47.5°$ lat and the respective subsequent 3 days. We acknowledge that with this approach we can only relate rainfall events close to the coastline to ARs. Based on these selected days, we ran a network analysis using ES (with the parameters $\tau_{\text{min}} = 0$, $\tau_{\text{max}} = 3$). Therefore, we investigate the immediate synchronization pattern of heavy rainfall events occurring simultaneously with ARs.

In Fig. 4 we show the resulting network divergence which is characterized by a large area of positive values at the coast overland and negative values over the eastern part of the Pacific. Note that network divergence is computed by subtracting *out_degree* $-$ *in_degree*. Therefore, areas with positive values have more outgoing links (sources) and areas with negative values have more incoming links (sinks). We identify a clear source in the Pacific ocean and a sink close to the western coast

https://doi.org/10.5194/egusphere-2022-530
Preprint. Discussion started: 29 June 2022
© Author(s) 2022. CC BY 4.0 License.

of NA. We find, that rainfall events over the Pacific occur first (and are therefore shown as sources), followed by rainfall events over the western parts of NA (hence these regions are marked as sinks). Additionally, it seems as if there is a wave-like pattern hidden in Fig. 4 (moving further east, we observe another large area of negative network divergence, followed by positive values over the Atlantic and the NA east coast). Since our filtering only allows for interpreting the dynamics near the western coast of NA, we can only speculate about the causes of this pattern. We suspect that there are either other climate features such as synchronized ARs serving as rainfall sources in the North (e. g. as described in Mo and Lin (2019)) or a previous AR strike that caused a cascade of synchronized heavy rainfall events traversing eastwards.

3.4 Synchronization of heavy rainfall events in the aftermath of AR events

After the proof of concept in the previous section, we now extend the spatial and temporal domain. Our initial analysis showed that heavy rainfall events which occur in central and eastern Canada, are synchronized with AR strikes at the western coast considering delays in a window between $\tau_{min} = 3$ and $\tau_{max} = 12$ (See Fig. 2). To now link heavy rainfall events that are triggered by ARs, we choose the following setup: we consider events that occurred from 0 to 12 days after the land-falling of an AR of at least category 3 and employ ES with $\tau_{min} = 3$ and $\tau_{max} = 12$. With that, we assure that we keep heavy rainfall events at the coastline and in central and eastern Canada, but only allow synchronization for temporal delays larger than 3 days. With that, we avoid obtaining a strong signal of synchronized events mainly along the western coast of NA (where the main synchronization of events happens during the first 3 days after the first AR day). In other words: we examine the delayed synchronization pattern of heavy rainfall events (at least 3 days between events) occurring at any time after the land-falling of an intense AR. The resulting network divergence is displayed in Fig. 5a.

We identify a region of positive network divergence along the northern part of the western coast of NA and especially a region of reduced network divergence over central and eastern Canada, where the synchronization between the AR time series and the heavy rainfall events was initially discovered. To finally verify that there is a strong connection between the North American west coast, where we find a large number of outgoing links, and central and eastern Canada, where many links terminate, we analyze where links that connect to central and eastern Canada originated (see out degree and red box in Fig. 5b).

Fig. 5b highlights the grid cells where links originate that terminate in Central and eastern Canada (red box). This box has been chosen based on where we have found the synchronization between the AR time series and the heavy rainfall time series (see Fig. 2 and Fig. 3). One main source of links to this region is the North and Northeast of the study area. This confirms that links emerge from the region that is marked by positive values in the network divergence (where heavy rainfall events synchronized within the first 3 days of an AR strike) and terminate in the red box.

In summary, we have identified a cascade of heavy rainfall events: in the first 3 days after the first day of an AR strike, rainfall events are mostly occurring close to or at the coast and synchronize in this area. In the subsequent days, moisture can be transported to central and eastern Canada and cause heavy rainfall there. This takes place between 3 and 12 days after the first AR-induced rainfall at the coastline.

https://doi.org/10.5194/egusphere-2022-530
Preprint. Discussion started: 29 June 2022
© Author(s) 2022. CC BY 4.0 License.

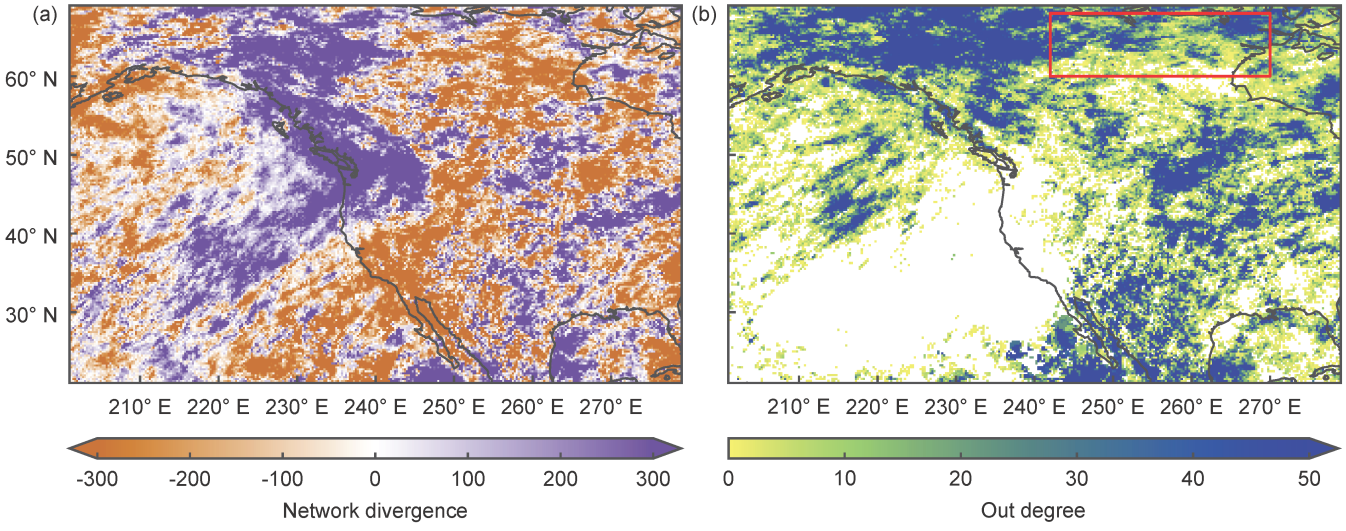

Figure 5. Network analysis based on the event synchronization (ES) between heavy rainfall and ARs of category 3 or higher that land-fell at latitudes $\geq 47.5^{\circ}$ according to the SIO-R1 catalog. We consider all rainfall events that occurred from 0 to 12 days after the land-falling of an AR and we calculate ES with $\tau_{min} = 3$ and $\tau_{max} = 12$. In the networks, only nodes with significantly directed event synchronization strength were connected (see Sect. 2 for more details). (a) Network divergence. Color bar as in Fig. 4. (b) Out degree of a directed network. Highlighted are the grid cells where links terminating in Central and eastern Canada originated (red box). This box was chosen based on the region with synchronization between the AR time series and the heavy rainfall time series found in Fig. 2 and Fig. 3.

3.5 Climatic conditions facilitating AR-induced heavy rainfall in central and eastern Canada

Measuring the synchronization between time series revealed the spatial extent as well as the temporal dimensions of rainfall related to ARs. To examine the climatic drivers leading to the heavy rainfall in central and eastern Canada, which is relatively far away from the location where the ARs land-fall, we study different climatological variables.

First, we show IVT anomalies on days with active ARs of category 3 or higher. Additionally, we investigate how the IVT anomalies develop over the respective subsequent days. The high IVT in Fig. 6 (top row) is a clear footprint of the ARs. Even after 5 days (right column), there is moisture influx related to the (by then) weakening ARs. The moisture is distributed further to the mainland the higher the delay, but with decreasing intensity.

Second, the 500 hPa geopotential height is assessed for varying delays as for the IVT in the second row of Fig. 6. The strong positive anomalies over the coastline indicate the position of the cyclonic storm causing the AR and the heavy rainfall along the coast. With a higher delay, the storm disintegrates slowly while shifting eastwards. Simultaneously, the negative anomalies mainly in the northwestern part of the study area (which correspond to high-pressure areas) also degenerate.

Third, the upper-level (250 hPa) meridional wind anomalies again for the AR-days and the subsequent days are displayed in the third row of Fig. 6. We observe a strong upper-level northward (southward) wind anomaly over the Pacific (continent). The meridional wind anomalies show the slow disintegration of the cyclonic storm but with a configuration that can guide moisture

https://doi.org/10.5194/egusphere-2022-530
Preprint. Discussion started: 29 June 2022
© Author(s) 2022. CC BY 4.0 License.

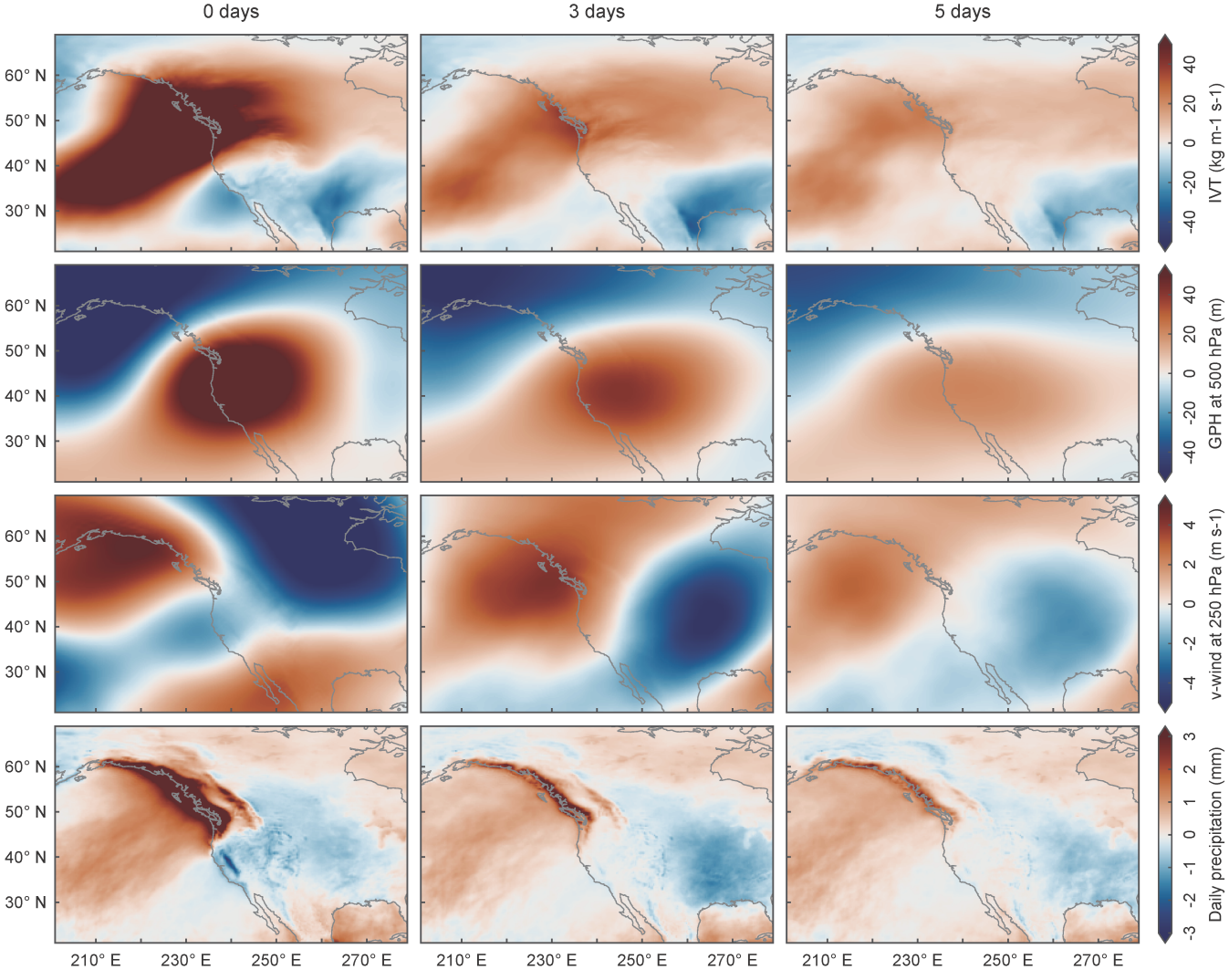

Figure 6. IVT (top row), geopotential height (second row), meridional wind (third row), and rainfall (bottom row) anomalies, from 0 (left column), 3 (middle column), and 5 (right column) days after the first day of land-falling of an AR of category 3 or higher over the western coast of NA at locations north of 47.5°N according to the SIO-R1 catalog.

https://doi.org/10.5194/egusphere-2022-530
Preprint. Discussion started: 29 June 2022
© Author(s) 2022. CC BY 4.0 License.

towards the northern parts of the continent, where we observe the synchronization of the AR time series and the heavy rainfall events.

Finally, we show rainfall anomalies based on the same parameter setting in the fourth row of Fig. 6. As ARs listed in the employed SIO-R1 catalog land-fall over the western coast, the main region of high rainfall anomalies is close to the west coast of NA. For increasing delay, we observe positive rainfall anomalies in central and eastern Canada, where we have found the synchronization of the AR time series and the heavy rainfall events. This is in line with the IVT anomaly which maintains an elevated level for higher delays.

4 Conclusions

In this study, we have investigated the influence of ARs on the large-scale spatio-temporal synchronization patterns of heavy rainfall over North America (NA). For this purpose, we have first analyzed if there is a significant association between ARs land-falling at the western coast of NA and heavy rainfall events over the coastal and continental regions. Employing event synchronization (ES), we have revealed timescale-dependent spatial patterns of heavy rainfall which are significantly correlated with AR strikes: i) immediately after an AR hits the coast, heavy rainfall events synchronize over the coastal areas. ii) Then, from 3 days after the land-fall, the synchronization close to the coast decreases significantly and only heavy rainfall events associated with more persistent ARs remain. iii) From 3 to 12 days after the first day of an AR strike, heavy rainfall events in central and eastern Canada synchronize with ARs that land-fell north of $47.5°$N. These results have been reproduced using an alternative AR catalog, establishing the robustness of our findings.

After examining the synchronization of heavy rainfall with singular AR time series, we have analyzed the organization of heavy rainfall during and after AR strikes. For this, we have evaluated ES between the time series of heavy rainfall events at different locations and for different temporal lags after the land-fall of the ARs. Based on that, we have first constructed a complex network considering a time window from 0 to 3 days after the land-fall of ARs. This result confirmed the common knowledge about ARs, namely that heavy rainfall events occurring simultaneously with ARs synchronize initially over the eastern part of the Pacific Ocean and then are followed by synchronous heavy rainfall events close to the western coast of NA. By examining a second complex network based on heavy rainfall events occurring at any time after the land-fall of an intense AR, but only allowing synchronization with a delay from 3 to 12 days, we have uncovered a strong connection between heavy rainfall events at the North American west coast and at central and eastern Canada: the moisture of the land-falling ARs along the coast can be transported to central and eastern Canada and cause heavy rainfall there.

To further investigate this result, we have studied the climatic conditions facilitating AR-induced heavy rainfall in central and eastern Canada. We have constructed the anomalies of vertically integrated water vapor transport (IVT), geopotential height at 500 hPa, upper-level meridional wind, and rainfall, on days with active ARs of category 3 or higher and the respective subsequent 3 and 5 days. We have found that IVT can penetrate the continent and reach the northern part of NA, maintaining a moisture influx even 5 days after the land-fall of the ARs. The 500 hPa geopotential height and the meridional wind anomalies showed a circulation pattern that can guide moisture towards the northern parts of the continent. Finally, for increasing delays,

https://doi.org/10.5194/egusphere-2022-530
Preprint. Discussion started: 29 June 2022
© Author(s) 2022. CC BY 4.0 License.

we have observed positive rainfall anomalies in central and eastern Canada, where the synchronization of the AR event time series and the heavy rainfall events has been found.

In summary, we have studied the spatio-temporal synchronization pattern of heavy rainfall induced by ARs, revealing its extent and its temporal evolution. We have shown that the impact of ARs hitting the western coast of NA is not limited to these areas, since they can be accompanied by delayed but significantly synchronized heavy rainfall events in the continental regions. In particular, we have identified a cascade of heavy rainfall events: in the first 3 days after the first day of an AR strike, heavy rainfall occurs along the coast. In the subsequent days, this moisture can be transported to central and eastern Canada and cause heavy rainfall there. Our results illustrate the role of ARs for distributing heavy rainfall over NA and should be considered to better anticipate the evolution of the climate dynamics of the region in the context of a warming atmosphere, where we expect a higher frequency and strength of ARs. Since our filtering with the AR time series only allowed us for interpreting the dynamics near the western coast of NA, the physical process by which moisture transported from the coast to the north of the continent causes rainfall there has not yet been identified. Future work could, for example, focus on singular cases of rainfall cascades to uncover the exact mechanisms and provide predictive power for heavy precipitation events in central and eastern Canada triggered by ARs hitting the western coast of NA.

Code and data availability. The code is available from the authors upon request. The analysis was conducted with Python and supported by the Python package Pyunicorn Donges et al. (2015). All data sets are publicly available. The ERA5 reanalysis data sets can be downloaded at https://cds.climate.copernicus.eu/. The SIO R1 Catalog can be accessed via https://weclima.ucsd.edu/data-products/.

Author contributions. FW wrote the manuscript with the help of SV. FW conducted the analysis. SV prepared the figures with the help of FW. DT prepared the section and table for the IPART catalog. All authors reviewed and improved the manuscript.

Competing interests. The authors declare that they have no competing interests.

Acknowledgements. This research has been funded by the BMBF grant climXtreme (No. 01LP1902J) “Spatial synchronization patterns of heavy precipitation events” and by DFG research training group GRK 2043/1 “Natural risk in a changing world (NatRiskChange)”. NB acknowledges funding from the Volkswagen Foundation.

https://doi.org/10.5194/egusphere-2022-530
Preprint. Discussion started: 29 June 2022
© Author(s) 2022. CC BY 4.0 License.

Appendix A

A1 Analyzing the impact of latitudinally categorized ARs.

In the main manuscript, we have only used ARs land-falling at latitudes $\geq 47.5°$. We have based that on the finding that the number of grid cells at which heavy rainfall time series are significantly correlated with the AR time series is not increasing for including ARs land-falling at lower latitudes. For that, we have step-wise included more ARs (with a $2.5°$ stepsize) and counted the number of significant grid cells in central and eastern Canada (for the spatial extent, see red box in Fig. 5b). As an illustration of how the results appear for including all ARs, we have run the analysis evaluating the synchronization between the heavy rainfall time series and the time series of ARs hitting the western coast of NA somewhere. We show Fig. A1, featuring otherwise the same results as Fig. 2.

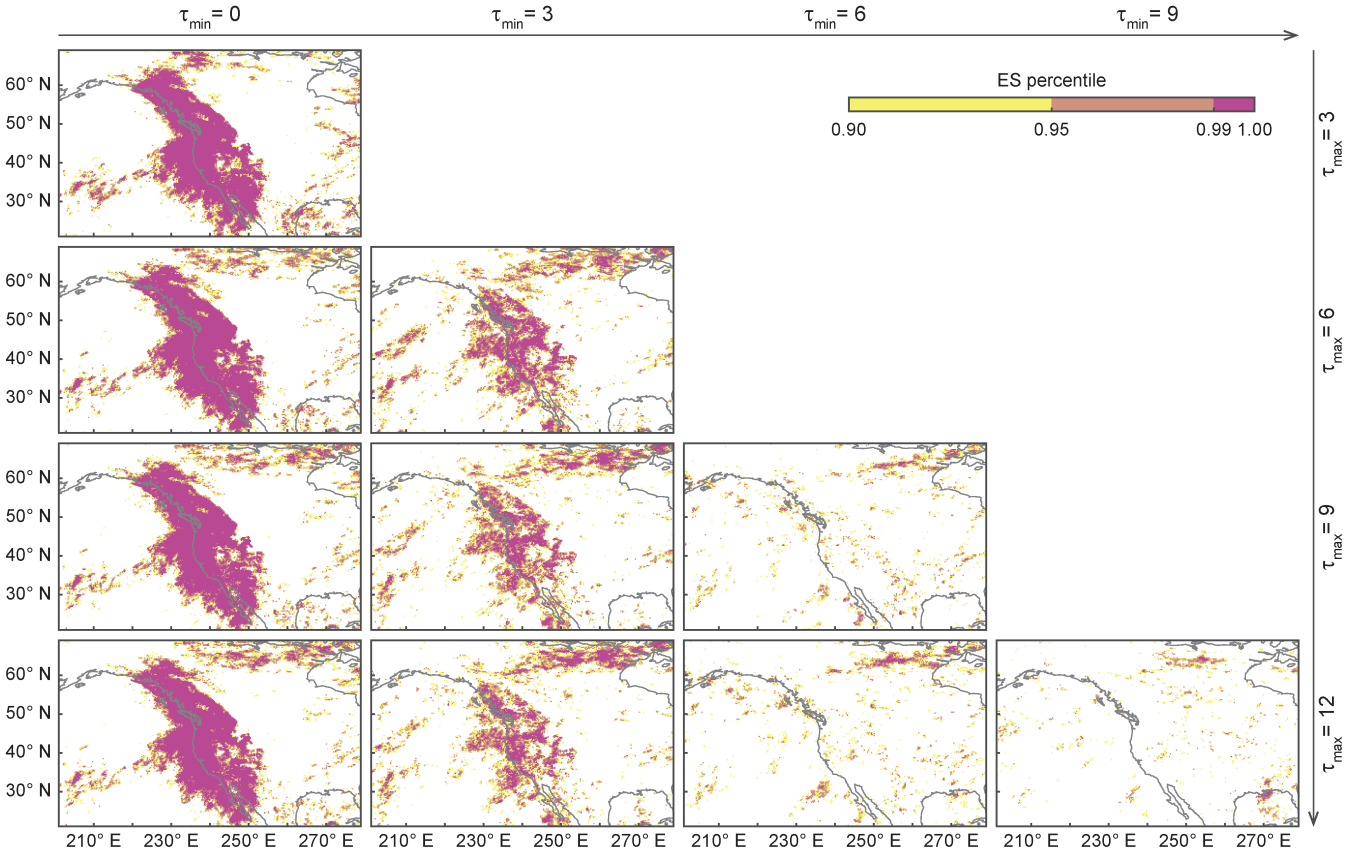

Figure A1. Event synchronization (ES) between time series of heavy rainfall events and the AR time series of the SIO-R1 catalog, considering all ARs of category 3 and higher that land-fell on the western coast of NA. Different values of τ_{min} and τ_{max} were considered to calculate ES in each panel: τ_{min} increases from left to right and τ_{max} from top to bottom. Color bar as in Fig. 2.

https://doi.org/10.5194/egusphere-2022-530
Preprint. Discussion started: 29 June 2022
© Author(s) 2022. CC BY 4.0 License.

As the results shown in Fig. A1 and Fig. 2 are neither visually distinguishable in central and eastern Canada nor does the number of grid points exhibiting significant synchronization increase, we assume our choice is robust and proceeded with the subset of ARs for the main analysis.

A2 Dependence on the choice of the AR catalog

As mentioned in the introduction, a plethora of work has analyzed how the choice of an AR detection algorithm affects the outcome of an analysis. For this reason, we have re-run the whole analysis for a systematically different AR catalog (for details see Sect. 2). Whereas in the main manuscript we have utilized the SIO-R1 catalog by Gershunov et al. (2017), here we feature the analysis carried out with a catalog based on the IPART algorithm (Xu et al., 2020).

To verify that we find, in principle, the same results using this alternative approach, we again show the results of assessing the synchronization between the AR time series and the heavy rainfall time series, this time for all ARs hitting the western coast of NA somewhere. The results are shown in Fig. A2. As expected, the results are visibly different to some extent and we have to acknowledge that we had to adapt the parameters of the analysis. In particular, for the IPART catalog, we reduced the considered lower threshold for the AR category. Therefore, Fig. A2 is based on ARs of category 2 and higher, whereas Fig. A1, Fig. 2 and Fig. 3 are based on ARs of category 3 and higher. We assume that this is due to two reasons: first, the ARs identified by the IPART catalog have, on average, a shorter persistence in comparison to the ones listed by the SIO-R1 catalog. Therefore, the ARs are often categorized higher (persistence is one criterion on the AR scale by Ralph et al. (2019)). Second, the IPART algorithm identified significantly fewer ARs, which leads to a more sparse AR time series. Then, filtering out many ARs may decrease the ES score due to the sparsity of the time series.

Aside from this adaptation, which we consider reasonable, we again, as before, find a region of synchronization between the heavy rainfall time series and the AR time series in central and eastern Canada. Note that the results show striking qualitative similarity (the signal is strongest for $\tau_{min} \geq 3$ and $\tau_{max} = 12$), and for $\tau_{min} \geq 3$ the signal close to the coast vanishes/gets less significant). Therefore, we consider the results based on the IPART catalog (Fig. A2) comparable to the results featured in the main manuscript (Fig. 2 and Fig. 3).

To be transparent regarding the construction of the IPART catalog we refer to Xu et al. (2020) and the chosen parameters below, which are mostly the default parameters of the algorithm.

https://doi.org/10.5194/egusphere-2022-530
Preprint. Discussion started: 29 June 2022
© Author(s) 2022. CC BY 4.0 License.

Table A1. Parameters used to create the IPART AR catalog.

Parameter name	Short description of the parameter	Parameter value	Unit	Step of the IPART algorithm
kernel	List of integers specifying the shape of the structuring element used in the gray erosion process	[16, 6, 6]	-	Top-hat by Reconstruction computation on IVT data
shift_lon	Shifts data along longitude dimension	80	degrees longitude	Top-hat by Reconstruction computation on IVT data
thres_low	Define AR candidates as regions >= this anomalous IVT	1	$kgm^{-1}s^{-1}$	Detect AR appearances from Top-hat by Reconstruction output
min_area	Drop AR candidates smaller than this area	500.000	km^2	Detect AR appearances from Top-hat by Reconstruction output
max_area	Drop AR candidates larger than this area	18.000.000	km^2	Detect AR appearances from Top-hat by Reconstruction output
min_LW	Minimal length to width ratio	2	-	Detect AR appearances from Top-hat by Reconstruction output
min_lat	Exclude ARs whose centroids are lower than this latitude	20	degrees latitude	Detect AR appearances from Top-hat by Reconstruction output
max_lat	Exclude ARs whose centroids are higher than this latitude	80	degrees latitude	Detect AR appearances from Top-hat by Reconstruction output
min_length	ARs shorter than this length are treated as relaxed	2,000	km	Detect AR appearances from Top-hat by Reconstruction output
min_length_hard	ARs shorter than this length are discarded	1,500	km	Detect AR appearances from Top-hat by Reconstruction output
rdp_thres	Error when simplifying axis using rdp algorithm	2	degrees latitude/longitude	Detect AR appearances from Top-hat by Reconstruction output
fill_radius	Number of grids as radius to fill small holes in AR contour	4	-	Detect AR appearances from Top-hat by Reconstruction output
single_dome	Do peak partition or not, used to separate systems that are merged together with an outer contour	False	-	Detect AR appearances from Top-hat by Reconstruction output
edge_eps	Minimal proportion of flux component in a direction to total flux to allow edge building in that direction	0.4	-	Detect AR appearances from Top-hat by Reconstruction output
zonal_cyclic	Whether to treat the data as zonally cyclic	True	-	Detect AR appearances from Top-hat by Reconstruction output
TIME_GAP_ALLOW	Gap allowed to link 2 ARs	6	hours	Track ARs at individual time steps to form tracks
TRACK_SCHEME	Tracking scheme	simple	-	Track ARs at individual time steps to form tracks
MAX_DIST_ALLOW	Maximal Hausdorff distance to define a neighborhood relationship	1200	km	Track ARs at individual time steps to form tracks
MIN_DURATION	Minimal duration to keep a track	0	hours	Track ARs at individual time steps to form tracks
MIN_NONRELAX	Minimal number of non-relaxed records in a track to keep a track.	0	-	Track ARs at individual time steps to form tracks

https://doi.org/10.5194/egusphere-2022-530
Preprint. Discussion started: 29 June 2022
© Author(s) 2022. CC BY 4.0 License.

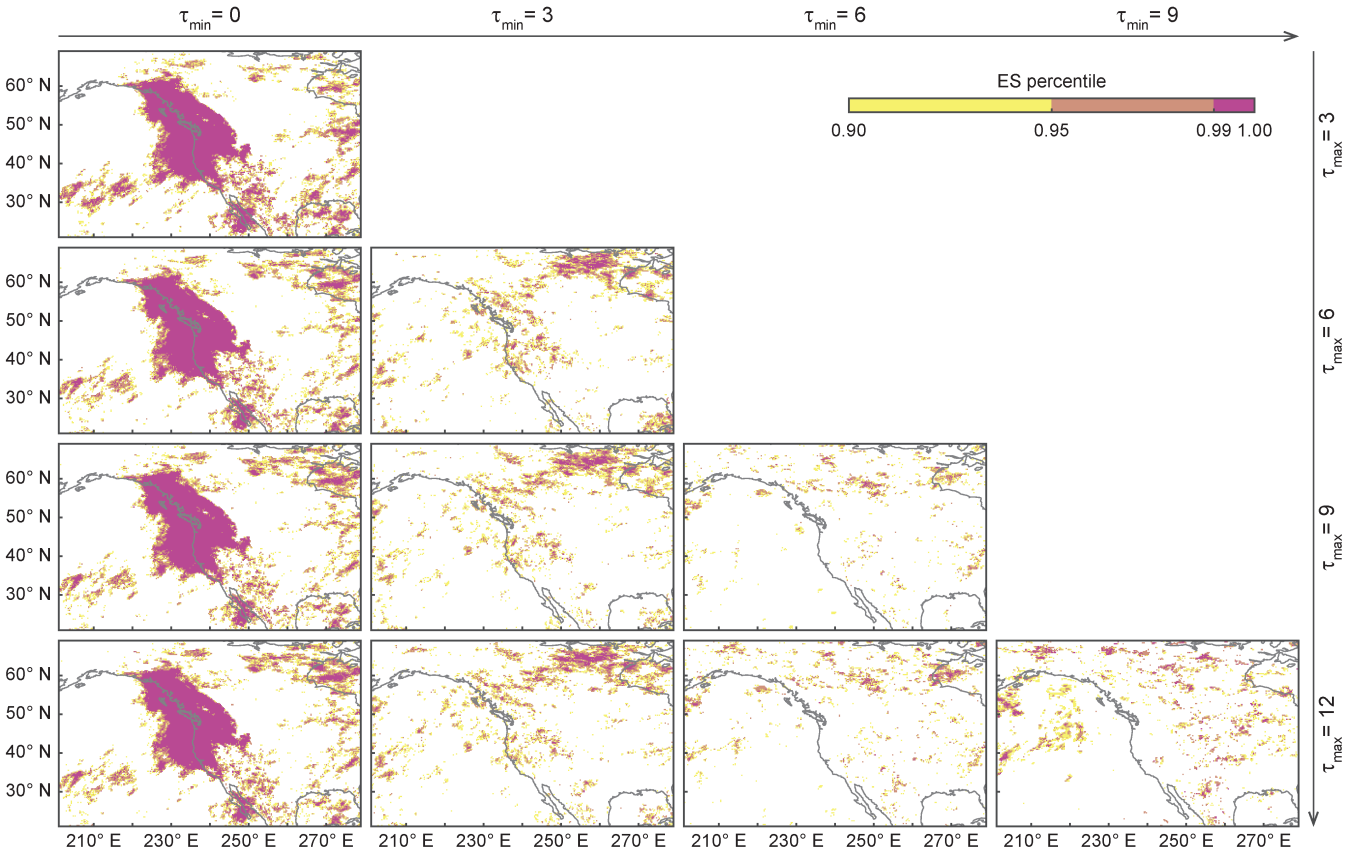

Figure A2. Event synchronization (ES) between time series of heavy rainfall events and the AR time series of the IPART catalog, considering all ARs of category 2 and higher that land-fell on the western coast of NA. Different values of τ_{min} and τ_{max} were considered to calculate ES in each panel: τ_{min} increases from left to right and τ_{max} from top to bottom. Color bar as in Fig. 2.

A3 Rainfall anomalies for increasing AR categories

As stated in the main manuscript, only considering ARs of category 4 and higher or even only examining only category 5 ARs does not lead to significant correlation between the AR time series and the heavy rainfall events. We suspect that first, the sparsity of the time series does not allow for significant ES scores but also that heavy rainfall events do not *only* occur after such strong ARs. To give an argument that these ARs still contribute to the heavy rainfall events, we studied the rainfall anomalies in the aftermath of just these exceptional AR events. The results are shown in Fig. A3.

Here, as in Fig. 6, the delay grows from left to right and the intensity increases from top to bottom. As there are only a few events, the pattern differs visibly between the different parameter settings, but nearly all configurations show a considerable signal of above-average rainfall in central and eastern Canada. Therefore, we conclude that these strong AR events are one

https://doi.org/10.5194/egusphere-2022-530
Preprint. Discussion started: 29 June 2022
© Author(s) 2022. CC BY 4.0 License.

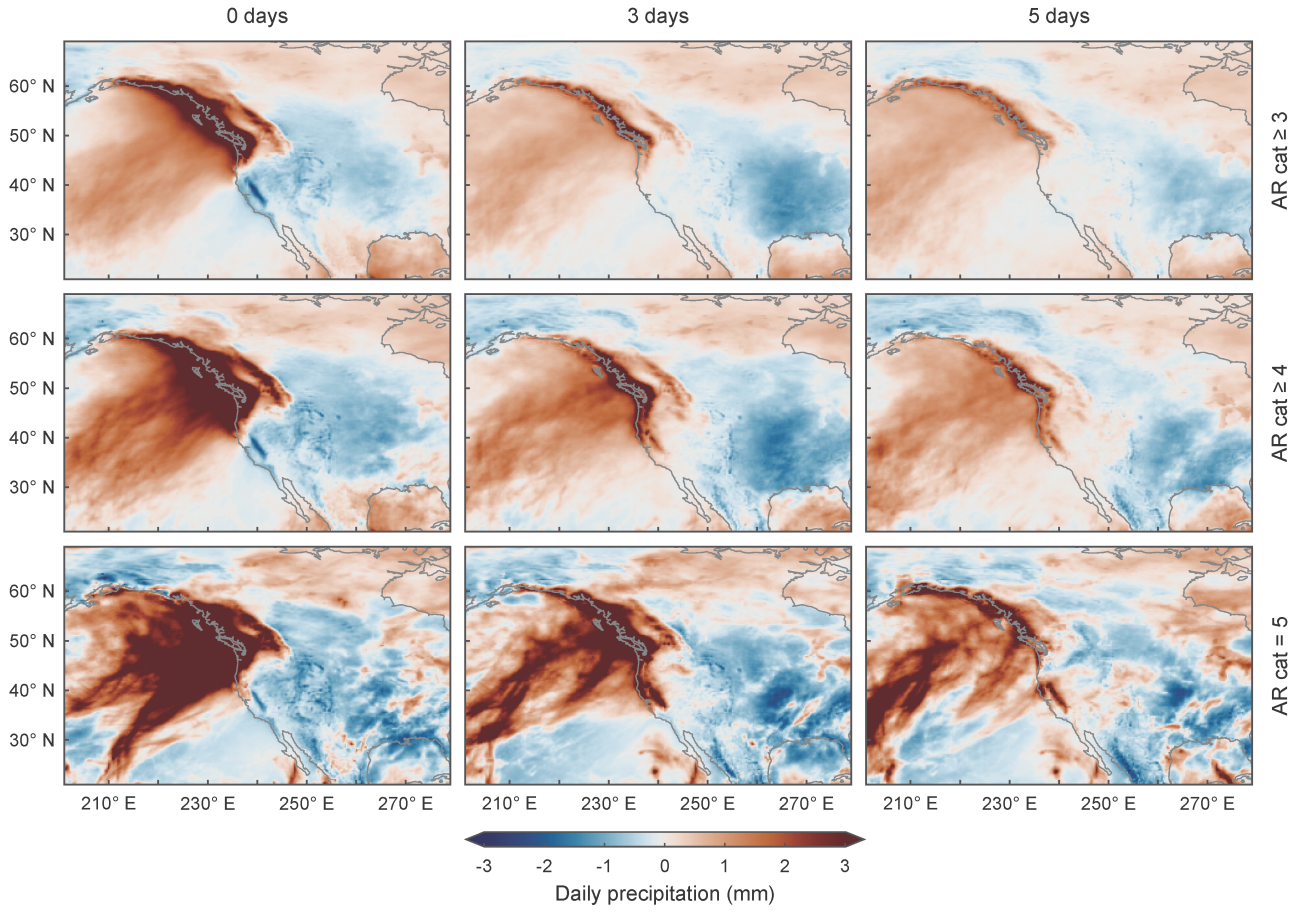

Figure A3. Rainfall anomalies, from 0 (left column), 3 (middle column), and 5 (right column) days after the first day of land-falling of an AR of category 3 or higher (top row), category 4 or higher (middle row), and category 5 (bottom row). We only consider ARs land-falling at locations north of 47.5°N according to the SIO-R1 catalog.

integral part of the found rainfall scheme but explain only one puzzle piece and, thus, do not explain, just by themselves, the increased rainfall in central and eastern Canada.

https://doi.org/10.5194/egusphere-2022-530
Preprint. Discussion started: 29 June 2022
© Author(s) 2022. CC BY 4.0 License.

References

Agarwal, A., Marwan, N., Ozturk, U., and Maheswaran, R.: Unfolding Community Structure in Rainfall Network of Germany Using Complex Network-Based Approach, Springer Singapore, https://doi.org/10.1007/978-981-13-2038-5, 2019.

Baggett, C. F., Lee, S., and Feldstein, S.: An investigation of the presence of atmospheric rivers over the North Pacific during planetary-scale wave life cycles and their role in Arctic warming, J. Atmos. Sci., 73, 4329–4347, https://doi.org/10.1175/JAS-D-16-0033.1, 2016.

Baggett, C. F., Barnes, E. A., Maloney, E. D., and Mundhenk, B. D.: Advancing atmospheric river forecasts into subseasonal-to-seasonal time scales, Geophys. Res. Lett., 44, 7528–7536, https://doi.org/10.1002/2017GL074434, 2017.

Boers, N., Bookhagen, B., Marwan, N., Kurths, J., and Marengo, J. A.: Complex networks identify spatial patterns of extreme rainfall events of the South American Monsoon System, Geophys. Res. Lett., 40, 4386–4392, https://doi.org/10.1002/grl.50681, 2013.

Boers, N., Bookhagen, B., Barbosa, H. M. J., Marwan, N., Kurths, J., and Marengo, J. A.: Prediction of extreme floods in the eastern Central Andes based on a complex networks approach, Nat. Commun., 5, 5199, 2014.

Boers, N., Goswami, B., Rheinwalt, A., Bookhagen, B., Hoskins, B., and Kurths, J.: Complex networks reveal global pattern of extreme-rainfall teleconnections, Nature, 566, 373–377, https://doi.org/10.1038/s41586-018-0872-x, 2019.

Corringham, T. W., Martin Ralph, F., Gershunov, A., Cayan, D. R., and Talbot, C. A.: Atmospheric rivers drive flood damages in the western United States, Sci. Adv., 5, https://doi.org/10.1126/sciadv.aax4631, 2019.

Dettinger, M. D., Ralph, F. M., Das, T., Neiman, P. J., and Cayan, D. R.: Atmospheric rivers, floods and the water resources of California, Water, 3, 445–478, https://doi.org/10.3390/w3020445, 2011.

Donges, J. F., Zou, Y., Marwan, N., and Kurths, J.: The backbone of the climate network, EPL, 87, 48 007, 2009.

Donges, J. F., Heitzig, J., Beronov, B., Wiedermann, M., Runge, J., Feng, Q. Y., Stolbova, V., Donner, R. V., Marwan, N., Dijkstra, H. A., and Kurths, J.: Unified functional network and nonlinear time series analysis for complex systems science: The pyunicorn package, Chaos, 25, https://doi.org/10.1063/1.4934554, 2015.

ECMWF: ERA5: Fifth generation of ECMWF atmospheric reanalyses of the global climate, Copernicus Climate Change Service Climate Data Store (CDS), access: Feb 22 2021, 2021.

Eiras-Barca, J., Ramos, A. M., Pinto, J. G., Trigo, R. M., Liberato, M. L., and Miguez-Macho, G.: The concurrence of atmospheric rivers and explosive cyclogenesis in the North Atlantic and North Pacific basins, Earth Syst. Dyn., 9, 91–102, https://doi.org/10.5194/esd-9-91-2018, 2018.

Gao, Y., Lu, J., Leung, L. R., Yang, Q., Hagos, S., and Qian, Y.: Dynamical and thermodynamical modulations on future changes of landfalling atmospheric rivers over western North America, Geophys. Res. Lett., 42, 7179–7186, https://doi.org/10.1002/2015GL065435, 2015.

Gershunov, A., Shulgina, T., Ralph, F. M., Lavers, D. A., and Rutz, J. J.: Assessing the climate-scale variability of atmospheric rivers affecting western North America, Geophys. Res. Lett., 44, 7900–7908, https://doi.org/10.1002/2017GL074175, 2017.

Gershunov, A., Shulgina, T., Clemesha, R. E., Guirguis, K., Pierce, D. W., Dettinger, M. D., Lavers, D. A., Cayan, D. R., Polade, S. D., Kalansky, J., and Ralph, F. M.: Precipitation regime change in Western North America: The role of Atmospheric Rivers, Sci. Rep., 9, https://doi.org/10.1038/s41598-019-46169-w, 2019.

Guirguis, K., Gershunov, A., DeFlorio, M. J., Shulgina, T., Delle Monache, L., Subramanian, A. C., Corringham, T. W., and Ralph, F. M.: Four atmospheric circulation regimes over the North Pacific and their relationship to California precipitation on daily to seasonal timescales, Geophysical Research Letters, 47, e2020GL087 609, 2020.

https://doi.org/10.5194/egusphere-2022-530
Preprint. Discussion started: 29 June 2022
© Author(s) 2022. CC BY 4.0 License.

Hagos, S. M., Leung, L. R., Yoon, J.-h., Lu, J., and Gao, Y.: North America from the Large Ensemble, Geophys. Res. Lett., 43, 1357–1363, https://doi.org/10.1002/2015GL067392.Received, 2016.

Huang, H., Patricola, C. M., Bercos-Hickey, E., Zhou, Y., Rhoades, A., Risser, M. D., and Collins, W. D.: Sources of Subseasonal-To-Seasonal Predictability of Atmospheric Rivers and Precipitation in the Western United States, Journal of Geophysical Research: Atmospheres, 126, e2020JD034 053, 2021.

Krichak, S. O., Barkan, J., Breitgand, J. S., Gualdi, S., and Feldstein, S. B.: The role of the export of tropical moisture into midlatitudes for extreme precipitation events in the Mediterranean region, Theor. Appl. Climatol., 121, 499–515, https://doi.org/10.1007/s00704-014-1244-6, 2015.

Lavers, D. A. and Villarini, G.: The nexus between atmospheric rivers and extreme precipitation across Europe, Geophys. Res. Lett., 40, 3259–3264, https://doi.org/10.1002/grl.50636, 2013.

Lora, J. M., Shields, C., and Rutz, J.: Consensus and disagreement in atmospheric river detection: ARTMIP global catalogues, Geophysical Research Letters, 47, e2020GL089 302, 2020.

Malik, N., Bookhagen, B., Marwan, N., and Kurths, J.: Analysis of spatial and temporal extreme monsoonal rainfall over South Asia using complex networks, Clim. Dyn., 39, 971–987, https://doi.org/10.1007/s00382-011-1156-4, 2012.

Mo, R. and Lin, H.: Tropical–mid-latitude interactions: Case study of an inland-penetrating atmospheric river during a major winter storm over North America, Atmosphere-Ocean, 57, 208–232, 2019.

Mundhenk, B. D., Barnes, E. A., Maloney, E. D., and Baggett, C. F.: Skillful empirical subseasonal prediction of landfalling atmospheric river activity using the Madden–Julian oscillation and quasi-biennial oscillation, npj Clim. Atmos. Sci., 1, 19–21, https://doi.org/10.1038/s41612-017-0008-2, 2018.

Neiman, P. J., Ralph, F. M., Wick, G. A., Lundquist, J. D., and Dettinger, M. D.: Meteorological characteristics and overland precipitation impacts of atmospheric rivers affecting the West coast of North America based on eight years of SSM/I satellite observations, J. Hydrometeorol., 9, 22–47, https://doi.org/10.1175/2007JHM855.1, 2008.

Newman, M., Kiladis, G. N., Weickmann, K. M., Ralph, F. M., and Sardeshmukh, P. D.: Relative contributions of synoptic and low-frequency eddies to time-mean atmospheric moisture transport, including the role of atmospheric rivers, J. Clim., 25, 7341–7361, https://doi.org/10.1175/JCLI-D-11-00665.1, 2012.

Ozturk, U., Malik, N., Cheung, K., Marwan, N., and Kurths, J.: A network - based comparative study of extreme tropical and frontal storm rainfall over Japan, Clim. Dyn., 53, 521–532, https://doi.org/10.1007/s00382-018-4597-1, 2019.

O'Brien, T. A., Wehner, M. F., Payne, A. E., Shields, C. A., Rutz, J. J., Leung, L.-R., Ralph, F. M., Collow, A., Gorodetskaya, I., Guan, B., et al.: Increases in future AR count and size: Overview of the ARTMIP Tier 2 CMIP5/6 experiment, Journal of Geophysical Research: Atmospheres, 127, e2021JD036 013, 2022.

Payne, A. E., Demory, M.-E., Leung, L. R., Ramos, A. M., Shields, C. A., Rutz, J. J., Siler, N., Villarini, G., Hall, A., and Ralph, F. M.: Responses and impacts of atmospheric rivers to climate change, Nat. Rev. Earth Environ., 1, 143–157, https://doi.org/10.1038/s43017-020-0030-5, 2020.

Quiroga, R. Q., Kreuz, T., and Grassberger, P.: Event synchronization: A simple and fast method to measure synchronicity and time delay patterns, Phys. Rev. E, 66, 041 904, https://doi.org/10.1103/PhysRevE.66.041904, 2002.

Ralph, F. M. and Dettinger, M. D.: Storms, floods, and the science of atmospheric rivers, Eos (Washington. DC)., 92, 265–266, https://doi.org/10.1029/2011EO320001, 2011.

https://doi.org/10.5194/egusphere-2022-530
Preprint. Discussion started: 29 June 2022
© Author(s) 2022. CC BY 4.0 License.

Ralph, F. M., Rutz, J. J., Cordeira, J. M., Dettinger, M., Anderson, M., Reynolds, D., Schick, L. J., and Smallcomb, C.: A scale to characterize the strength and impacts of atmospheric rivers, Bull. Am. Meteorol. Soc., 100, 269–289, https://doi.org/10.1175/BAMS-D-18-0023.1, 2019.

Ramos, A. M., Nieto, R., Tomé, R., Gimeno, L., Trigo, R. M., Liberato, M. L., and Lavers, D. A.: Atmospheric rivers moisture sources from a Lagrangian perspective, Earth Syst. Dyn., 7, 371–384, https://doi.org/10.5194/esd-7-371-2016, 2016.

Rutz, J. J., Shields, C. A., Lora, J. M., Payne, A. E., Guan, B., Ullrich, P., O'brien, T., Leung, L. R., Ralph, F. M., Wehner, M., et al.: The atmospheric river tracking method intercomparison project (ARTMIP): quantifying uncertainties in atmospheric river climatology, Journal of Geophysical Research: Atmospheres, 124, 13 777–13 802, 2019.

Sharma, A. R. and Déry, S. J.: Contribution of Atmospheric Rivers to Annual, Seasonal, and Extreme Precipitation Across British Columbia and Southeastern Alaska, J. Geophys. Res. Atmos., 125, 1–21, https://doi.org/10.1029/2019JD031823, 2020.

Shields, C. A. and Kiehl, J. T.: Atmospheric river landfall-latitude changes in future climate simulations, Geophysical Research Letters, 43, 8775–8782, 2016.

Shields, C. A., Rutz, J. J., Leung, L.-Y., Ralph, F. M., Wehner, M., Kawzenuk, B., Lora, J. M., McClenny, E., Osborne, T., Payne, A. E., et al.: Atmospheric river tracking method intercomparison project (ARTMIP): project goals and experimental design, Geoscientific Model Development, 11, 2455–2474, 2018.

Smith, B. L., Yuter, S. E., Neiman, P. J., and Kingsmill, D. E.: Water vapor fluxes and orographic precipitation over northern california associated with a landfalling atmospheric river, Mon. Weather Rev., 138, 74–100, https://doi.org/10.1175/2009MWR2939.1, 2010.

Stolbova, V., Martin, P., Bookhagen, B., Marwan, N., and Kurths, J.: Topology and seasonal evolution of the network of extreme precipitation over the Indian subcontinent and Sri Lanka, Nonlinear Process. Geophys., 21, 901–917, https://doi.org/10.5194/npg-21-901-2014, 2014.

Tsonis, A. A. and Roebber, P. J.: The architecture of the climate network, Phys. A, 333, 497–504, 2004.

Tsonis, A. A., Swanson, K. L., and Roebber, P. J.: What do networks have to do with climate?, Bull. Am. Meteorol. Soc., 87, 585–595, 2006.

Waliser, D. and Guan, B.: Extreme winds and precipitation during landfall of atmospheric rivers, Nat. Geosci., 10, 179–183, https://doi.org/10.1038/ngeo2894, 2017.

Warner, M. D., Mass, C. F., and Salathe Jr, E. P.: Changes in winter atmospheric rivers along the North American west coast in CMIP5 climate models, Journal of Hydrometeorology, 16, 118–128, 2015.

Wolf, F. and Donner, R. V.: Spatial organization of connectivity in functional climate networks describing event synchrony of heavy precipitation, The European Physical Journal Special Topics, pp. 1–19, https://doi.org/0.1140/epjs/s11734-021-00166-1, 2021.

Wolf, F., Bauer, J., Boers, N., and Donner, R. V.: Event synchrony measures for functional climate network analysis : A case study on South American rainfall dynamics Event synchrony measures for functional climate network analysis : A case study on South American rainfall dynamics, Chaos, 30, 033 102, https://doi.org/10.1063/1.5134012, 2020a.

Wolf, F., Ozturk, U., Cheung, K., and Donner, R. V.: Spatiotemporal patterns of synchronous heavy rainfall events in East Asia during the Baiu season, Earth Syst. Dyn. Discuss., https://esd.copernicus.org/preprints/esd-2020-69/, 2020b.

Xu, G., Ma, X., and Chang, P.: IPART: A Python Package for Image-Processing based Atmospheric River Tracking, Journal of Open Source Software, 5, 2407, https://doi.org/10.21105/joss.02407, 2020.

Zhang, Z., Ralph, F. M., and Zheng, M.: The relationship between extratropical cyclone strength and atmospheric river intensity and position, Geophysical Research Letters, 46, 1814–1823, 2019.

Zhou, Y., O'Brien, T. A., Ullrich, P. A., Collins, W. D., Patricola, C. M., and Rhoades, A. M.: Uncertainties in Atmospheric River Lifecycles by Detection Algorithms: Climatology and Variability, Journal of Geophysical Research: Atmospheres, 126, e2020JD033 711, 2021.

https://doi.org/10.5194/egusphere-2022-530
Preprint. Discussion started: 29 June 2022
© Author(s) 2022. CC BY 4.0 License.

Zhu, Y. and Newell, R. E.: A proposed algorithm for moisture fluxes from atmospheric rivers, Mon. Weather Rev., 126, 725–735, https://doi.org/10.1175/1520-0493(1998)126<0725:APAFMF>2.0.CO;2, 1998.